



Effective boundary conditions for buoyancy-driven flows and heat transfer in fully open-ended two-dimensional enclosures

K. Khanafer, K. Vafai *

Department of Mechanical Engineering, The Ohio State University, Columbus, OH 43210, USA

Received 10 May 2001; received in revised form 29 October 2001

Abstract

The present work achieves an accurate representation of the effective boundary conditions at the aperture plane of a two-dimensional open-ended structure for wide range of pertinent parameters. The presented effective boundary conditions are correlated in terms of Rayleigh number, Prandtl number, and the aspect ratio of the open-ended geometry. The numerical procedure used in this work is based on the Galerkin weighted residual method of finite-element formulation. Comprehensive comparisons between the present investigation using the effective boundary conditions for the anticipated closed-ended model and the results for the fully extended computational domain confirm successful implementation of the proposed model. Implementation of this representation reduces the main difficulties associated with specifying the open-ended boundary conditions and results in very substantial savings in CPU and memory usage. The present work plays an important role on modeling a basic and generic set of effective boundary conditions at the aperture plane for several applications of practical interest. © 2002 Elsevier Science Ltd. All rights reserved.

Keywords: Natural convection; Two-dimensional; Open-ended structure; Effective boundary conditions

1. Introduction

Natural convection in open-ended cavities has received considerable attention by many researchers both experimentally and numerically. This attention stems from the importance of such geometry in solar receiver systems, fire research, electronic cooling, brake housing of an aircraft, and many environmental geothermal processes. Most of the studies in this area have been aimed at two-dimensional analysis of rectangular cavities.

Bejan and Kimura [1] conducted both theoretical and experimental studies to investigate the penetration of natural convection into a horizontal cavity. It was

shown theoretically that the flow consists of a horizontal counter flow that penetrates the cavity over a distinct length, which is proportional to the cavity height and the square root of the Rayleigh number. In addition, it was also shown that the Nusselt number for the cavity is proportional to the square root of the Rayleigh number and is relatively unaffected by the Prandtl number. The theoretical results were validated by a flow visualization experiment.

Penot [2] conducted a numerical study of two-dimensional natural convection in an isothermal open square enclosure. The governing equations were solved in an enlarged computational domain by utilizing the far field boundary conditions. The effect of inclination and Grashof number were studied in this investigation. Two kinds of unsteady motion were observed inside the cavity. One was isothermal in nature and occurs for Grashof numbers higher than 10^5 for a vertical cavity. The other instability is hydrodynamic and existed for an upward facing cavity. In this case, the lower wall acts as an independent inclined flat plate, producing an up-

* Corresponding author. Present address: Department of Mechanical Engineering, University of California, Riverside, A 363 Bourns Hall, Riverside, CA 92521-0425, USA. Tel.: 1-909-787-2135; fax: 1-909-787-2899.

E-mail address: vafai@engr.ucr.edu (K. Vafai).

Nomenclature			
A	aspect ratio of the enclosure ($A = w/H$)	Θ	dimensionless temperature
H	height of the enclosure, m	u	velocity in the x direction, m s^{-1}
L_x	extended computational domain length in x -direction, m	v	velocity in the y direction, m s^{-1}
L_y	extended computational domain length in y -direction, m	U	dimensionless velocity in the x -direction
n	outward normal to a surface	V	dimensionless velocity in the y -direction
Nu	Nusselt number	w	width of the enclosure, m
p	pressure, Pa	x, y	cartesian coordinates, m
P	dimensionless pressure	<i>Greek symbols</i>	
Pr	Prandtl number (ν/α)	α	thermal diffusivity, $\text{m}^2 \text{s}^{-1}$
q	heat flux vector	β	coefficient of volume expansion, K^{-1}
Ra	Rayleigh number ($g\beta H^3 \Delta T / \nu \alpha$)	μ	dynamic viscosity, $\text{kg m}^{-1} \text{s}^{-1}$
T	temperature, $^\circ\text{C}$	ν	kinematic viscosity, $\text{m}^2 \text{s}^{-1}$
T_w	enclosure wall temperature, $^\circ\text{C}$	ρ	density, kg m^{-3}
		<i>Subscripts</i>	
		∞	condition at infinity
		w	wall of the enclosure

ward-directed flow. This flow is in conflict with the main flow penetrating inside the cavity. This unsteadiness was observed for low Grashof numbers. The same configuration with variable properties using primitive variables was studied by LeQuere et al. [3]. The authors in this investigation demonstrated that the flow unsteadiness takes place for large values of Grashof number and the penetration of the flow field into the open cavity depends on the far field boundary conditions. The effect of cavity aspect ratio, cavity inclination, inside wall temperature, and Grashof number was studied. Unsteady flow was observed inside the cavity for Grashof numbers higher than 10^6 . The results of this investigation showed that the thermal losses diminished with an increase of the inclination angle. This due to stable stratification of the flow and decreased unsteadiness. It was also shown that an increase in the inner wall temperature resulted in enhanced heat transfer rates from the top wall while reducing the losses from the lower wall. The overall heat transfer rates from the cavity were found to increase with an increase in the values of Grashof numbers and aspect ratios.

Other problems involving two-dimensional natural convection in open enclosures were studied by Doria [4] for predicting fire spread in a room and by Jacobs et al. [5,6] in modeling circulation above city streets and geothermal reservoirs. Experimental studies were also done by Humphrey and co-workers [7] and Sernas and Kyriakides [8] in modeling solar systems. Sernas and Kyriakides [8] studied two-dimensional, laminar natural convection in an open cavity filled with air as a working fluid with cavity aspect ratio of unity. The results of this study showed that the heat flux distribution and the velocity profiles along the inner vertical hot wall agreed well with the analytical results for an

isothermal vertical flat plate at the same Grashof number.

Experimental results for natural convection in a rectangular enclosure were illustrated by Hess and Henze [9]. The flow fields in both fully open and partially open cavities were studied by using laser doppler velocimetry. The Rayleigh numbers used in this investigation were in the range 3×10^{10} – 2×10^{11} . The vertical wall of the enclosure was maintained at a uniform high temperature while the top and bottom surfaces were kept insulated. For partially open cavity, the results showed that the transition to turbulence was found to occur at local Rayleigh numbers of 2×10^{10} – 3×10^{10} .

Chan and Tien [10] performed a numerical steady-state study of laminar natural convection in a two-dimensional square open cavity with a heated vertical wall and two insulated horizontal walls. Calculations were made in an extended computational domain beyond the aperture plane for cavity with a heated vertical wall and two horizontal insulated walls. Results obtained for Rayleigh numbers ranging from 10^3 to 10^9 were found to approach those of natural convection over a vertical isothermal flat plate. Later on, the same authors [11] conducted a numerical study for a two-dimensional, shallow rectangular open enclosure for Rayleigh numbers up to 10^6 . The computational domain was restricted to the cavity region and approximate boundary conditions were applied directly at the aperture plane. This approach did not predict some of the important features of the flow field near the aperture plane of the cavity since the corner and outer regions were not included in the analysis.

Chan and Tien [12] performed an experimental study for natural convection in a two-dimensional open rectangular cavity. Water was used as the working fluid in

this experiment. It was observed at low Rayleigh numbers that the fluid exits the cavity as a buoyant “plume” while at higher Rayleigh numbers, the exit velocities are high enough to form a buoyant “jet”. The effect of the open boundary was found to consist of two parts: the outgoing hot fluid exhibiting strong characteristics of the cavity conditions and incoming flow influenced by the outside conditions.

A comprehensive study was conducted by Vafai and Etefagh [13] for investigating basic aspects and physics of the flow field within the open-ended structures and the effect of extended computational domain on flow and heat transfer inside the open-ended cavity and its immediate surroundings. They demonstrated that the required extent of the enlarged computational domain for obtaining accurate results was much larger than that shown by previous investigators. In addition, they showed that the far field flow characteristics were sensitive to the type of boundary conditions used. The transient behavior of the flow field through the formation of vortices and the opposing interactions of the buoyant and suction mechanisms leading to an oscillating central vortex were analyzed. Their study also included the effect of the Rayleigh number, Prandtl number, temperature ratio (between the upper and lower blocks), and the aspect ratio of the cavity. The thermal and fluid flow instabilities in natural convection in open-ended cavities were analyzed by Vafai and Etefagh [14]. They showed, at higher Rayleigh numbers, the existence of periodic oscillations in the Nusselt number correspond to the central vortex’s oscillations and its location inside the cavity. The frequency of these oscillations was found to increase linearly with the Rayleigh number.

Although for a closed cavity it is possible to specify the boundary conditions on all the boundaries of the enclosure, the main difficulty associated with the study of fluid flow in open-ended structure is the specification of the boundary conditions at the open end. Most numerical studies of open cavities rely on solving the governing equations in a domain extended outside the opening side of the enclosure and applying the far field conditions at the boundary of the extended domain due to lack of known physical boundary conditions at the aperture plane. Vafai and Etefagh [13,14] have shown that the extent of the extended computational domain must be much larger than previously utilized and as such they have shown substantial inaccuracies associated with the later approach.

The extension of the open-ended domain requires substantially larger memory and computational time. An appropriate set of effective boundary conditions at the aperture plane of the open-ended structure will drastically reduce the storage capacity and the CPU requirements of the computer resources. Recently, Khanafer and Vafai [15] conducted a comprehensive study for the elimination of the extended boundaries in

open-ended structures for both two- and three-dimensional geometries. An accurate set of effective boundary conditions for both the flow and the temperature fields was obtained covering a range of Rayleigh numbers and aspect ratios for a partially open-ended geometry for the fixed value of Prandtl number ($Pr = 0.71$). The authors showed that the use of the presented two- and three-dimensional closed-ended models results in substantial savings in CPU and memory usage while producing results which are shown to compare very well with the fully extended models. This has a great advantage when dealing with complex problems that require large CPU time such as fire research, energy conservation in buildings, and cooling of aircraft brakes. As a result, there is a need to have approximate yet fairly accurate boundary conditions at the open side of the geometry.

The present work focuses on modeling an accurate representation for a basic and generic set of effective boundary conditions for two-dimensional open-ended structure at both ends (open-ended sides). In this approach, the velocity and temperature variations at the aperture plane (open-ended side) are correlated in terms of the controlling parameters for a wide range of Rayleigh number, aspect ratio, and Prandtl numbers. This will give the present correlations an advantage over the other approximate boundary conditions in the literature. Such approximate boundary conditions at any plane should be represented by the physical parameters of the problem since these parameters have a significant effect on the accuracy of any approximate boundary conditions. The numerical simulations will be carried out using both an extended outer computational domain through the implementation of the far field boundary conditions as well as elimination of the extended domain through an appropriate use of the effective boundary conditions thus reducing the problem to a closed-ended geometry.

2. Physical model and assumptions

Consider the two-dimensional open-ended cavity shown in Fig. 1(a). It should be noted that due to symmetry consideration, half of the open-ended cavity is used in the present study as shown in Fig. 1(b). The validity of using the symmetry conditions at the centerline of the cavity was checked through a series of numerical runs. The coordinate system for the open-ended enclosure under consideration is illustrated in Fig. 1. This model is similar to the configuration used by Vafai and Etefagh [13]. The lower and upper walls of the enclosure are maintained at constant temperatures T_w , while the surrounding fluid communicating with the open-ended geometry is at an ambient temperature T_∞ , which is lower than T_w . The problem is modeled as a two-dimensional, incompressible, steady natural con-

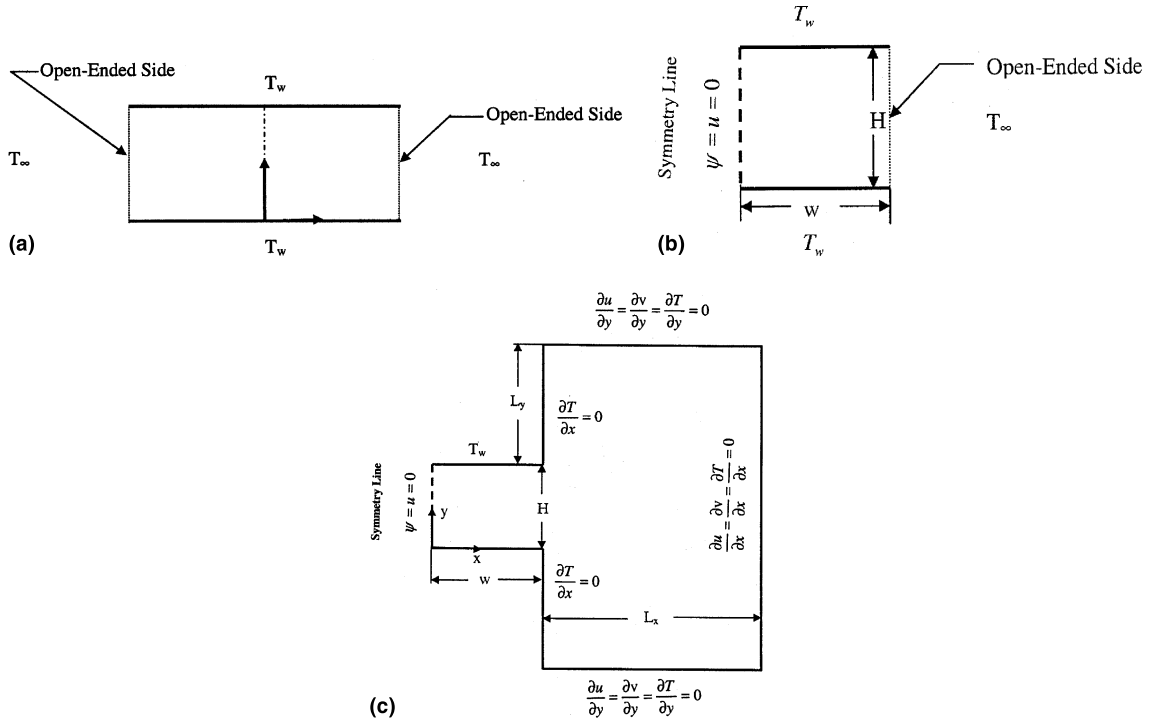


Fig. 1. (a) Physical domain, (b) physical domain utilizing the symmetry condition, and (c) computational domain utilizing the symmetry condition.

vection. The fluid physical properties are assumed constant and the Boussinesq approximation is invoked.

The physical governing equations for the present problem are based on the balance laws for mass, linear momentum, and thermal energy. Taking into account the above-mentioned assumptions, these equations, expressed in non-dimensional form, can be written as

$$\frac{\partial U}{\partial X} + \frac{\partial V}{\partial Y} = 0, \tag{1}$$

$$\sqrt{\frac{Ra}{Pr}} \left(U \frac{\partial U}{\partial X} + V \frac{\partial U}{\partial Y} \right) = - \frac{\partial P}{\partial X} + \left(\frac{\partial^2 U}{\partial X^2} + \frac{\partial^2 U}{\partial Y^2} \right), \tag{2}$$

$$\sqrt{\frac{Ra}{Pr}} \left(U \frac{\partial V}{\partial X} + V \frac{\partial V}{\partial Y} \right) = - \frac{\partial P}{\partial Y} + \left(\frac{\partial^2 V}{\partial X^2} + \frac{\partial^2 V}{\partial Y^2} \right) + \sqrt{\frac{Ra}{Pr}} \Theta, \tag{3}$$

$$\sqrt{\frac{Ra}{Pr}} \left(U \frac{\partial \Theta}{\partial X} + V \frac{\partial \Theta}{\partial Y} \right) = \frac{\partial^2 \Theta}{\partial X^2} + \frac{\partial^2 \Theta}{\partial Y^2}. \tag{4}$$

The resultant three non-dimensional parameters in the above equations are the Rayleigh number defined as $Ra = g\beta H^3 \Delta T / \nu \alpha$, the Prandtl number, $Pr = \nu / \alpha$, and the aspect ratio, $A = w / H$.

Eqs. (1)–(4) were made dimensionless by using a proper set of scaling parameters:

$$X = \frac{x}{H}, \quad Y = \frac{y}{H},$$

$$U = \frac{uH}{\alpha \sqrt{RaPr}}, \quad V = \frac{vH}{\alpha \sqrt{RaPr}}, \quad P = \frac{pH^2}{\mu \alpha \sqrt{RaPr}}, \tag{5}$$

$$\Theta = \frac{T - T_\infty}{\Delta T}, \quad \Delta T = T_w - T_\infty.$$

In the above equations, u and v are the velocity components in the x - and y -directions, T is the fluid temperature, p is the fluid pressure, β is the volumetric expansion coefficient, H is the height of the enclosure, T_w is the enclosure wall temperature, and ν , μ , and c_p are the kinematic viscosity, dynamic viscosity, and the specific heat, respectively.

2.1. Boundary conditions

The boundary conditions on the extended computational domain based on the analysis present in Vafai and Ettfagh [13,14] can be written as

(I) For the left wall of the enclosure at $x = 0$ (Symmetry line)

$$u = \psi = \frac{\partial v}{\partial x} = \frac{\partial T}{\partial x} = 0. \tag{6}$$

(II) For the upper and lower walls of the enclosure at $y = 0, H$

$$u = v = 0 \quad \text{and} \quad T = T_w. \tag{7}$$

(III) For the x -far field open boundaries $x = L_x + w$ and $-L_y \leq y \leq L_y + H$

$$\frac{\partial T}{\partial x} = \frac{\partial v}{\partial x} = \frac{\partial u}{\partial x} = 0. \tag{8}$$

(IV) For the y -far field open boundaries at $y = -L_y, L_y + H$ and $w \leq x \leq L_x + w$

$$\frac{\partial T}{\partial y} = \frac{\partial v}{\partial y} = \frac{\partial u}{\partial y} = 0. \tag{9}$$

3. Numerical scheme

A Galerkin-based FEM is employed to solve the governing equations for the present study. The application of this technique is well described by Taylor and Hood [16] and Gresho et al. [17], and its application is

also well documented [18]. The segregated solution algorithm is utilized to solve the system of equations. The advantage of using this method is that the global system matrix is decomposed into smaller submatrices and then solved in a sequential manner. This technique will result in considerably fewer storage requirements. The conjugate residual scheme is used to solve the symmetric pressure type equation systems, while the conjugate gradient squared is used for the non-symmetric advection–diffusion type equations. Extensive numerical experimentation was performed to attain grid-independent results for all the field variables.

4. Heat transfer calculations

In the present investigation, the local Nusselt number is defined as

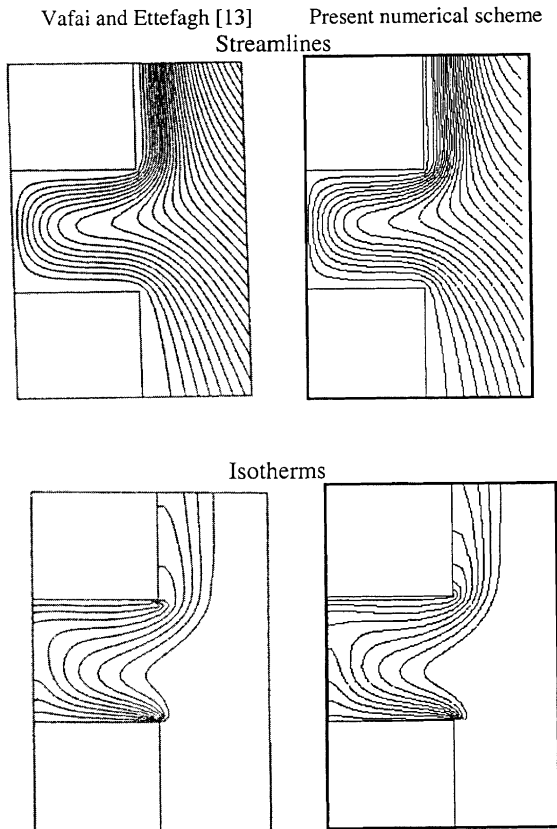


Fig. 2. Comparison of the streamlines and isotherms between the two-dimensional model utilizing the extended boundaries and that of Vafai and Ettefagh [13] for Rayleigh number $Ra = 10^4$.

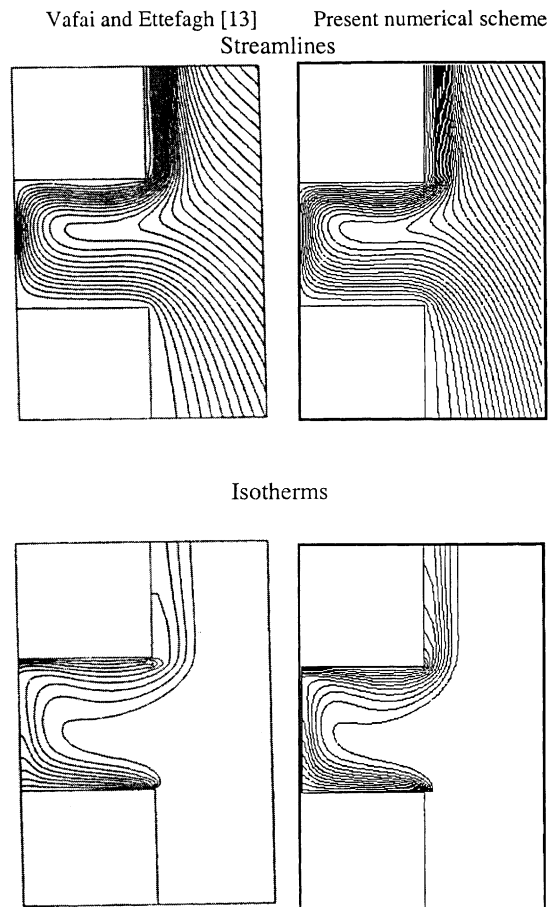


Fig. 3. Comparison of the streamlines and isotherms between the two-dimensional model utilizing the extended boundaries and that of Vafai and Ettefagh [13] for Rayleigh number $Ra = 10^5$.

Table 1
Comparison of the average Nusselt numbers between the present numerical scheme and the two dimensional results of Vafai and Ettefagh [13] for various Rayleigh numbers

	$Ra = 10^4$			$Ra = 10^5$		
	Present	Vafai and Ettefagh [13]	Percent diff. (%)	Present	Vafai and Ettefagh [13]	Percent diff. (%)
Nu (lower)	1.99	2.0	0.5	3.15	2.98	5.7
Nu (upper)	1.09	1.05	3.8	2.9	3.1	6.5

$$Nu = \frac{\partial \Theta}{\partial n}, \tag{10}$$

where n denotes the outward pointing normal from the surface over which the heat flux is calculated. This definition of the local Nusselt number is used to represent all the heat transfer results in the present study.

4.1. Model validation

The present numerical scheme is validated against the finite difference solution of Vafai and Ettefagh [13] for a wide range of Rayleigh number by utilizing the full ex-

tent of the extended boundaries. Figs. 2 and 3 show a very good agreement between the present work utilizing an extended domain and the results reported by Vafai and Ettefagh [13] for open-ended cavity with extended outer boundaries.

As an additional check on the accuracy of the present results, Table 1 shows a comparison of the Nusselt number measured at the top and bottom walls of the enclosure between the present numerical scheme and that of Vafai and Ettefagh [13] for different Rayleigh numbers. It can be seen from the table that both solutions are in excellent agreement.

Present model (using effective B.C's) Vafai and Ettefagh [13] (using far field B.C's)

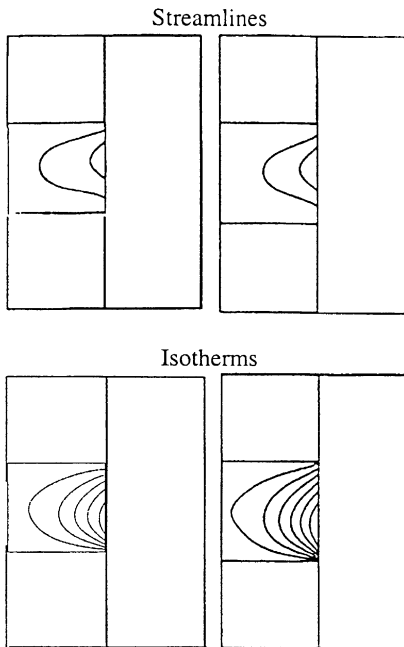


Fig. 4. Comparison of the streamlines and the isotherms between the present effective boundary conditions model and that of full model by Vafai and Ettefagh [13] for $Ra = 10^3$, $A = 1$, and $Pr = 0.71$.

Present model (using effective B.C's) Vafai and Ettefagh [13] (using far field B.C's)

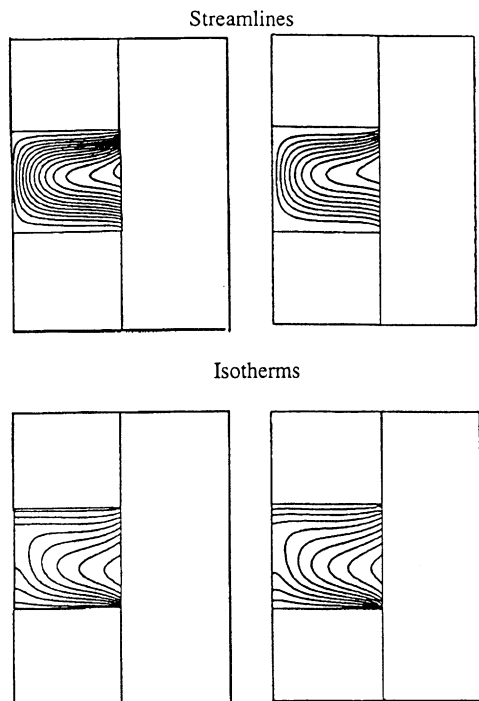


Fig. 5. Comparison of the streamlines and the isotherms between the present effective boundary conditions model and that of full model by Vafai and Ettefagh [13] for $Ra = 10^4$, $A = 1$, and $Pr = 0.71$.

5. Two-dimensional model based on effective boundary conditions

The physical governing equations for the present investigation are solved numerically for a wide range of pertinent parameters to obtain a set of appropriate effective boundary conditions for the velocity and temperature fields at the aperture plane of the two-dimensional enclosure. The effect of the outer extended boundaries was fully taken into account in this analysis. The results were then correlated in terms of the pertinent controlling parameters. These controlling parameters include the Rayleigh number, Prandtl number, and the aspect ratio of the enclosure. A wide range of Rayleigh numbers was selected for this investigation as $10^3 \leq Ra \leq 10^5$, Prandtl number was varied in the range of $0.7 \leq Pr \leq 7$. Also, a wide range of the aspect ratios, $A = w/H$ of the enclosure, was selected as $0.25 \leq A \leq 1$. For the two-dimensional open cavity case, after a detailed and comprehensive set of simulations, the effective boundary conditions at the

open side of the enclosure were found to be well presented by the following.

5.1. $10^3 \leq Ra \leq 10^4$

For the range of $0.75 \leq A \leq 1.0$, $0.71 \leq Pr \leq 1.5$, the field variables at the aperture side were found to be very well represented by

$$U = a_1 + a_2Y + a_3Y^2 + a_4Y^4 + a_5Y^5 + a_6Y^6 + a_7Ra + a_8(YRa) + a_9(YRa)^2 + a_{10}(YRa)^3,$$

where $a_1 = 0.00984$, $a_2 = -3.46899$,
 $a_3 = 11.78402$, $a_4 = -55.28402$,
 $a_5 = 89.7516$, $a_6 = -42.7625$,
 $a_7 = -8.72 \times 10^{-6}$, $a_8 = 2.539 \times 10^{-5}$,
 $a_9 = -2.65562 \times 10^{-9}$, $a_{10} = 2.0716 \times 10^{-13}$.

Present model (using effective B.C's) Full model (utilizing far field B.C's)

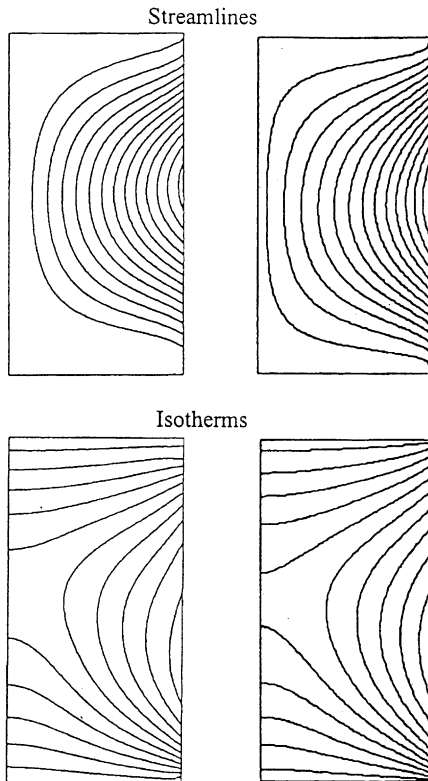


Fig. 6. Comparison of the streamlines and the isotherms between the present effective boundary conditions model and that of full model for $Ra = 10^3$, $A = 0.5$, and $Pr = 4.92$.

Present model (using effective B.C's) Full model (utilizing far field B.C's)

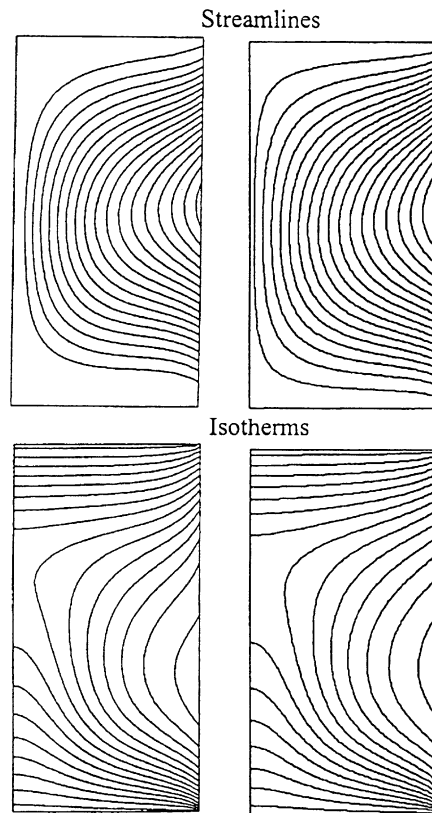


Fig. 7. Comparison of the streamlines and the isotherms between the present effective boundary conditions model and that of full model for $Ra = 5 \times 10^3$, $A = 0.5$, and $Pr = 4.92$.

$$V = b_1 + b_2 Y^5 + b_3 Y^6 + b_4 Ra^4 + b_5 (YRa) + b_6 (YRa)^2 + b_7 (YRa)^3 + b_8 (YPr) + b_9 (YPr)^2 + b_{10} (YPr)^3, \tag{11}$$

where $b_1 = 0.03294$, $b_2 = 2.99781$,
 $b_3 = -3.80476$, $b_4 = -1.806 \times 10^{-18}$,
 $b_5 = -5.518 \times 10^{-5}$, $b_6 = 8.0774 \times 10^{-9}$,
 $b_7 = -2.894 \times 10^{-13}$, $b_8 = 2.2522$,
 $b_9 = -9.38728$, $b_{10} = 11.19303$.

$$\Theta = c_1 + c_2 Y^2 + c_3 Y^4 + c_4 Y^5 + c_5 Ra^2 + c_6 (YA) + c_7 (YA)^3 + c_8 (YRa)^3 + c_9 (PrRa),$$

where $c_1 = 1.13266$, $c_2 = 25.93947$,
 $c_3 = 41.61256$, $c_4 = -13.98949$,
 $c_5 = 2.628386 \times 10^{-9}$, $c_6 = -7.17108$,
 $c_7 = -46.42616$, $c_8 = 1.58688 \times 10^{-13}$,
 $c_9 = -8.025 \times 10^{-5}$.

For the range of $0.25 \leq A \leq 0.5$, $1.5 \leq Pr \leq 7.0$, the field variables at the aperture side were found to be very well represented by

$$U = a_1 + a_2 Y + a_3 Y^5 + a_4 Y^6 + a_5 Pr^2 + a_6 (YA) + a_7 (YA)^2 + a_8 (YA)^3 + a_9 (YRa)^3 + a_{10} (YPr)^2,$$

where $a_1 = -0.08961$, $a_2 = 0.51137$,
 $a_3 = 1.34046$, $a_4 = -1.46304$,
 $a_5 = 0.00235$, $a_6 = -2.93232$,
 $a_7 = 10.84539$, $a_8 = -11.41043$,
 $a_9 = 5.135 \times 10^{-14}$, $a_{10} = -0.00698$.

$$V = b_1 + b_2 Y + b_3 Y^2 + b_4 Y^3 + b_5 Y^6 + b_6 A^4 + b_7 Ra^2 + b_8 (YA) + b_9 (YA)^2 + b_{10} (YRa) + b_{11} (YRa)^2 + b_{12} (YPr)^2$$

Present model (using effective B.C's) Full model (utilizing far field B.C's)

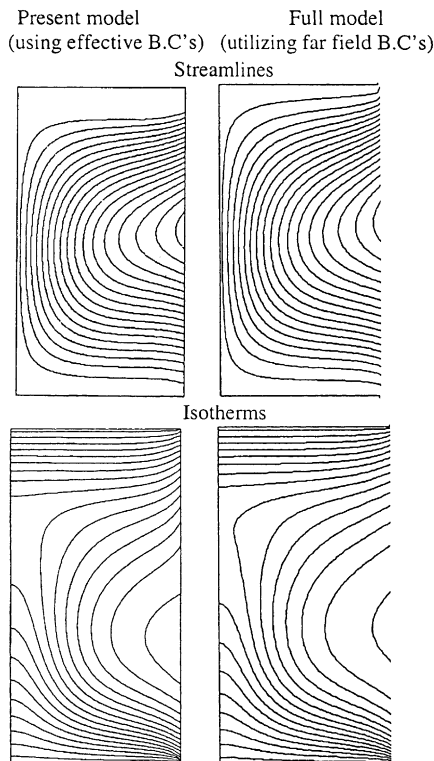
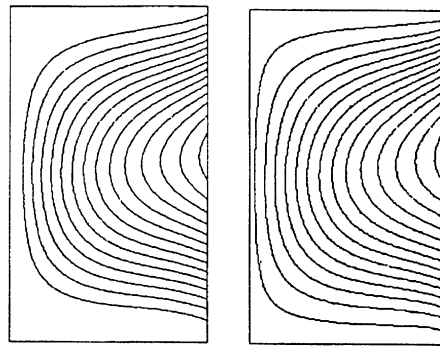


Fig. 8. Comparison of the streamlines and the isotherms between the present effective boundary conditions model and that of full model for $Ra = 10^4$, $A = 0.5$, and $Pr = 4.92$.

Streamlines



Isotherms

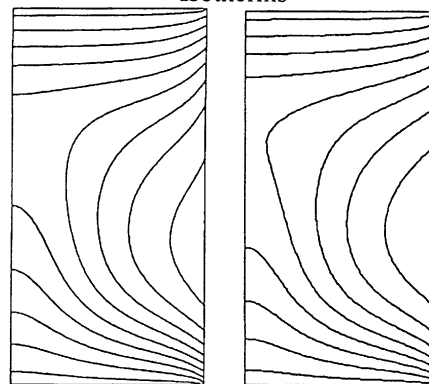


Fig. 9. Comparison of the streamlines and the isotherms between the present effective boundary conditions model and that of full model for $Ra = 5 \times 10^3$, $A = 0.5$, and $Pr = 2.5$.

$$+ b_{13}(ARa) + b_{14}(ARa)^2 + b_{15}(APr)^2 + b_{16}(RaPr) + b_{17}(RaPr)^2,$$

where $b_1 = -0.01332$, $b_2 = 1.20063$,
 $b_3 = -2.06295$, $b_4 = 1.73838$,
 $b_5 = -0.67042$, $b_6 = 1.2234$,
 $b_7 = -1.7948 \times 10^{-10}$, $b_8 = -1.22023$, (12)
 $b_9 = 1.69804$, $b_{10} = -1.09 \times 10^{-5}$,
 $b_{11} = 1.3357 \times 10^{-9}$, $b_{12} = -0.00111$,
 $b_{13} = -4.374 \times 10^{-5}$, $b_{14} = 3.480179 \times 10^{-9}$,
 $b_{15} = -0.00804$, $b_{16} = 5.31 \times 10^{-6}$,
 $b_{17} = -5.4756 \times 10^{-11}$.

$$\Theta = c_1 + c_2Y + c_3Y^2 + c_4Y^3 + c_5Y^4 + c_6Y^5 + c_7(YA)^3 + c_8(YRa)^3 + c_9(ARa) + c_{10}(ARa)^2,$$

where $c_1 = 1.15346$, $c_2 = -7.29914$,
 $c_3 = 26.01647$, $c_4 = -43.99807$,
 $c_5 = 34.55099$, $c_6 = -9.43208$,
 $c_7 = 1.58346$, $c_8 = 9.50159 \times 10^{-14}$,
 $c_9 = -1.4385 \times 10^{-4}$, $c_{10} = 1.498081 \times 10^{-8}$.

5.2. $10^4 \leq Ra \leq 10^5$

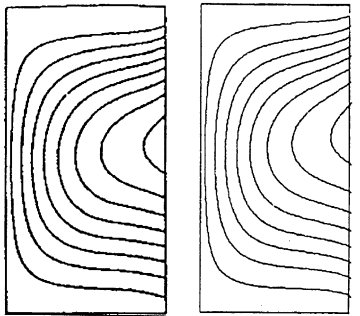
For the range of $0.75 \leq A \leq 1.0$ and $0.71 \leq Pr \leq 7.0$, the field variables at the aperture were found to be very well represented by

$$U = a_1 + a_2Y + a_3Y^2 + a_4Y^4 + a_5Y^5 + a_6Y^6 + a_7Pr^2 + a_8(YA) + a_9(YA)^2 + a_{10}(YRa) + a_{11}(YPr)^2 + a_{12}(YPr)^3,$$

where $a_1 = -0.08305$, $a_2 = -1.45324$,
 $a_3 = 8.33439$, $a_4 = -46.16284$,
 $a_5 = 76.10035$, $a_6 = -36.34571$,
 $a_7 = 0.00315$, $a_8 = -0.93987$,
 $a_9 = 0.75178$, $a_{10} = -2.71768 \times 10^{-7}$,
 $a_{11} = -0.01404$, $a_{12} = 0.00080843$

$$V = b_1 + b_2Y + b_3Y^2 + b_4Y^5 + b_5Y^6 + b_6Ra^4 + b_7(YA)^3 + b_8(YRa) + b_9(YRa)^2 + b_{10}(YPr)^3 + b_{11}(APr) + b_{12}(RaPr)^2 + b_{13}(RaPr)^3,$$

Present model (using effective B.C.'s) Full model (utilizing far field B.C.'s)
 Streamlines



Isotherms

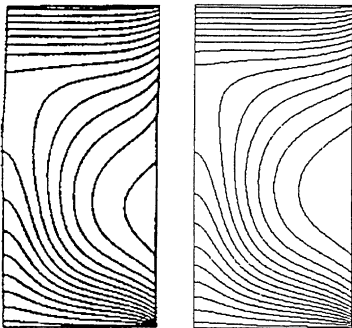
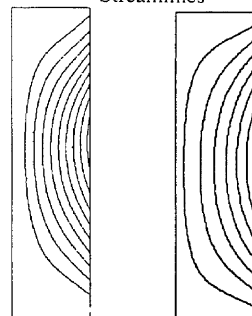


Fig. 10. Comparison of the streamlines and the isotherms between the present effective boundary conditions model and that of full model for $Ra = 1 \times 10^4$, $A = 0.5$, and $Pr = 2.5$.

Present model (using effective B.C.'s) Full model (utilizing far field B.C.'s)
 Streamlines



Isotherms

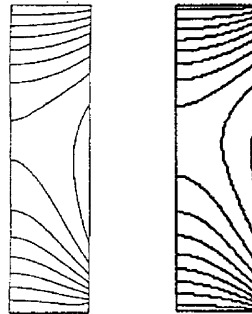


Fig. 11. Comparison of the streamlines and the isotherms between the present effective boundary conditions model and that of full model for $Ra = 1 \times 10^3$, $A = 0.25$, and $Pr = 3.5$.

where $b_1 = 0.06168$, $b_2 = 0.56029$,
 $b_3 = -1.54346$, $b_4 = 6.33908$, (13)
 $b_5 = -5.39448$, $b_6 = -7.5415 \times 10^{-22}$,
 $b_7 = 0.09886$, $b_8 = -2.22 \times 10^{-6}$,
 $b_9 = 2.1137 \times 10^{-11}$, $b_{10} = -2.8717 \times 10^{-4}$,
 $b_{11} = -0.01659$, $b_{12} = -8.9291 \times 10^{-12}$,
 $b_{13} = 3.30422 \times 10^{-16}$.

$$\Theta = c_1 + c_2 Y + c_3 Y^2 + c_4 Y^3 + c_5 Y^4 + c_6 Y^5 + c_7 Y^6 + c_8 (APr) + c_9 (RaPr),$$

where $c_1 = 1.01677$, $c_2 = -12.3993$,
 $c_3 = 68.02645$, $c_4 = -192.82469$,
 $c_5 = 290.4974$, $c_6 = -218.19187$,
 $c_7 = 64.91869$, $c_8 = 0.01441$,
 $c_9 = -1.85 \times 10^{-6}$.

The validity of the above effective boundary conditions (11)–(13) at the aperture plane of the open-ended enclosure was validated against both published results in the literature and with results obtained by utilizing the far field boundary conditions of the open-end cavity shown

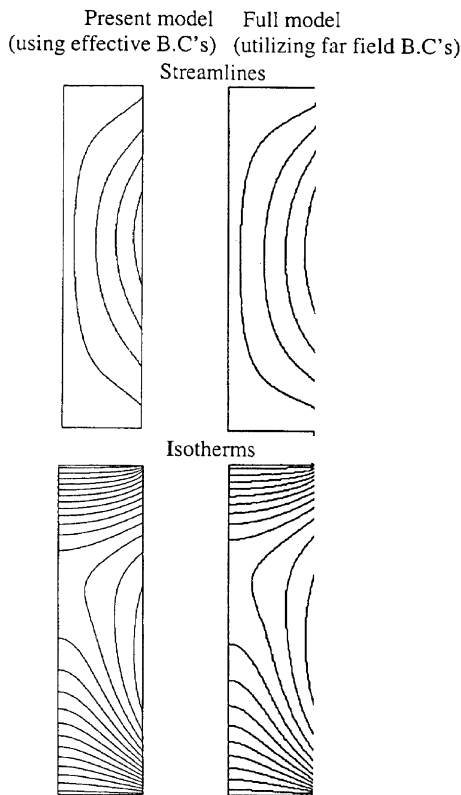


Fig. 12. Comparison of the streamlines and the isotherms between the present effective boundary conditions model and that of full model for $Ra = 5 \times 10^3$, $A = 0.25$, and $Pr = 3.5$.

in Fig. 1. The accuracy of the above effective boundary conditions is shown in Figs. 4–13. The present effective boundary conditions were validated against the work of Vafai and Etefagh [13]. These comparisons are shown in Figs. 4 and 5. These figures illustrate an excellent comparison of the isotherms and the streamlines between the present closed-ended model and the fully extended boundary model for various controlling parameters. Moreover, the accuracy of the above-mentioned effective boundary conditions were benchmarked against the results obtained by utilizing the far field boundary conditions for various physical parameters such as Rayleigh number, Prandtl number, and aspect ratio of the enclosure as shown in Figs. 6–13. These figures show that the effective boundary closed-ended model is in excellent agreement with the fully extended model.

An additional check on the accuracy of the present effective boundary conditions is made by comparing the upper and lower Nusselt numbers for both models at various controlling parameters as shown in Tables 2–5. The results for the Nusselt number were first verified with the results reported by Vafai and Etefagh [13] as shown in Table 2. It is clearly seen in this table that both the set of results are in very good agreement. In addition, the accuracy of the average upper and lower Nusselt numbers of the enclosure using the effective boundary conditions were verified

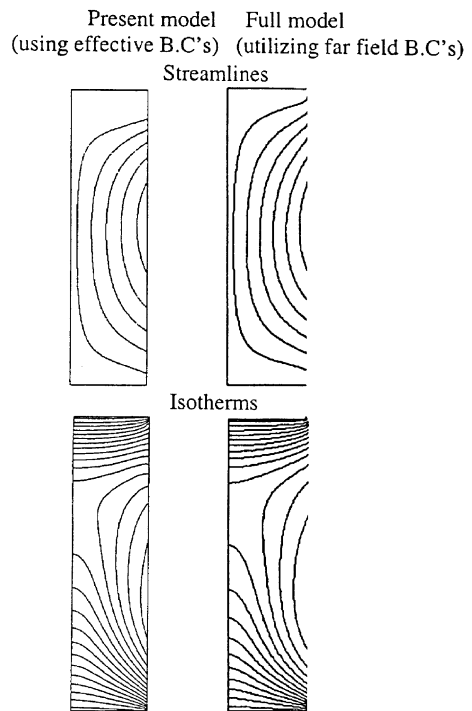


Fig. 13. Comparison of the streamlines and the isotherms between the present effective boundary conditions model and that of full model for $Ra = 1 \times 10^4$, $A = 0.25$, and $Pr = 3.5$.

Table 2

Comparison of the Nusselt numbers between the present model (no outer boundaries) and the results based on utilizing the fully extended outer boundaries ($A = 1, Pr = 0.71$)

$Ra \setminus Nu$	Present (with outer boundaries)	Present (closed-ended model)	Vafai and Ettefagh [13]
(a) Upper Nusselt number			
1×10^3	0.7554	0.676	0.806
5×10^3	1.4739	1.392	NA
1×10^4	2.1579	2.074	2.15
(b) Lower Nusselt number			
1×10^3	1.2547	1.2411	1.2415
5×10^3	2.5408	2.420	NA
1×10^4	3.1563	3.174	3.16

Table 3

Comparison of the Nusselt numbers between the present model (no outer boundaries) and the results based on utilizing the fully extended outer boundaries ($A = 0.5, Pr = 2.5$)

$Ra \setminus Nu$	Present (with outer boundaries)	Present (closed-ended model)	Percentage error (%)
(a) Upper Nusselt number			
1×10^3	1.64	1.49	9.15
5×10^3	2.97	2.90	2.03
1×10^4	4.04	3.82	4.5
(b) Lower Nusselt number			
1×10^3	2.13	1.97	7.51
5×10^3	3.51	3.36	4.27
1×10^4	4.20	4.21	0.24

Table 4

Comparison of the Nusselt numbers between the present model (no outer boundaries) and the results based on utilizing the fully extended outer boundaries ($A = 0.25, Pr = 3.5$)

$Ra \setminus Nu$	Present (with outer boundaries)	Present (closed-ended model)	Percentage error (%)
(a) Upper Nusselt number			
1×10^3	2.76	2.75	0.36
5×10^3	4.19	4.06	3.1
1×10^4	5.04	4.88	3.17
(b) Lower Nusselt number			
1×10^3	2.61	2.36	9.6
5×10^3	3.65	3.32	9.04
1×10^4	4.35	4.16	4.36

Table 5

Comparison of the Nusselt numbers between the present model (no outer boundaries) and the results based on utilizing the fully extended outer boundaries ($A = 0.5, Pr = 4.92$)

$Ra \setminus Nu$	Present (with outer boundaries)	Present (closed-ended model)	Percentage error (%)
(a) Upper Nusselt number			
1×10^3	1.59	1.48	6.92
5×10^3	2.83	2.83	0.0
1×10^4	3.83	3.52	8.09
(b) Lower Nusselt number			
1×10^3	2.09	1.99	4.78
5×10^3	3.50	3.52	0.57
1×10^4	4.38	4.39	0.23

Table 6

Comparison of the CPU time reduction for the two-dimensional model at various Rayleigh numbers and an aspect ratio of 1

Ra	CPU (with outer boundaries)	CPU (using effective boundary conditions)	Reduction (%)
1×10^3	76	9.0	88.2
5×10^3	85	7.0	91.8
1×10^4	178	6.13	96.6

against the results obtained by utilizing the fully extended model as shown in Fig. 1. The results were found to be in very good agreement as depicted in Tables 3–5.

The cited correlations in Eqs. (11)–(13) result in large reduction in CPU time and memory usage for simulations involving open-ended structures. The solution for the enlarged computational domain requires large CPU time and memory storage to overcome the problem of unknown boundary conditions for the open-ended region. Table 6 shows a substantial reduction in CPU time for two-dimensional model using the effective boundary conditions presented in Eqs. (11)–(13).

6. Conclusions

An accurate set of effective boundary conditions for flow and temperature fields at the aperture plane for two-dimensional open-ended structure was obtained for a wide range of pertinent parameters such as Rayleigh number, Prandtl number, and aspect ratio. Comprehensive comparisons for the streamlines and the isotherms within the enclosure were presented for various controlling parameters between the two-dimensional closed-ended model (based on the use of effective boundary conditions) and the fully extended domain utilizing the far field boundary conditions. The simulations demonstrated very good agreements between the two models. Moreover, detailed assessment of the average Nusselt number was carried out between the two models establishing the validity of the present effective boundary conditions. The implementation of the presented two-dimensional effective boundary conditions results in very substantial savings in CPU and memory usage. The present correlations represent a design tool for several applications of practical interest that require large CPU time

References

- [1] A. Bejan, S. Kimura, Penetration of free convection into a lateral cavity, *J. Fluid Mech.* 103 (1981) 465–478.
- [2] F. Penot, Numerical calculation of two-dimensional natural convection in isothermal open cavities, *Numer. Heat Transfer* 5 (1982) 421–437.
- [3] O. LeQuere, J.A.C. Humphery, F.S. Sherman, Numerical calculation of thermally driven two-dimensional unsteady laminar flow in cavities of rectangular cross section, *Numer. Heat Transfer* 4 (1981) 249–283.
- [4] M.L. Doria, A numerical model for the prediction of two-dimensional unsteady flows of multi-component gases with strong buoyancy effects and recirculation, Notre Dame Report, TR-37191-74-4, 1974.
- [5] H.R. Jacobs, W.E. Mason, W.T. Hikida, Natural convection in open rectangular cavities, in: *Proceedings of the Fifth International Heat Transfer Conference*, Tokyo, Japan, vol. 3, 1974, pp. 90–94.
- [6] H.R. Jacobs, W.E. Mason, Natural convection in open rectangular cavities with adiabatic sidewalls, in: *Proceedings of the 1976 Heat Transfer and Fluid Mechanics Institute*, Stanford University Press, Stanford, 1976, pp. 33–46.
- [7] K.S. Chen, J.A.C. Humphery, F.S. Sherman, Experimental investigation of thermally driven flow in open cavities of rectangular cross-section, *Philos. Trans. R. Soc. London A* 316 (1985) 57–84.
- [8] V. Serans, I. Kyriakides, Natural convection in an open cavity, in: *Proceedings of the Seventh International Heat Transfer Conference*, Munchen, Germany, vol. 2, 1982, pp. 275–286.
- [9] C.F. Hess, R.H. Henze, Experimental investigation of natural convection losses from open cavities, *J. Heat Transfer* 106 (1984) 333–338.
- [10] Y.L. Chan, C.L. Tien, A numerical study of two-dimensional natural convection in square open cavities, *Numer. Heat Transfer* 8 (1985) 65–80.
- [11] Y.L. Chan, C.L. Tien, A numerical study of two-dimensional laminar natural convection in shallow open cavities, *Int. J. Heat Mass Transfer* 28 (1985) 603–612.
- [12] Y.L. Chan, C.L. Tien, Laminar natural convection in shallow open cavities, *J. Heat Transfer* 108 (1986) 305–309.
- [13] K. Vafai, J. Etefagh, The effects of sharp corners on buoyancy-driven flows with particular emphasis on outer boundaries, *Int. J. Heat Mass Transfer* 33 (1990) 2311–2328.
- [14] K. Vafai, J. Etefagh, Thermal and fluid flow instabilities in buoyancy-driven flows in open-ended cavities, *Int. J. Heat Mass Transfer* 33 (1990) 2329–2344.
- [15] K. Khanafer, K. Vafai, Buoyancy-driven flows and heat transfer in open-ended enclosures: elimination of the extended boundaries, *Int. J. Heat Mass Transfer* 43 (2000) 4087–4100.
- [16] C. Taylor, P. Hood, A numerical solution of the Navier–Stokes equations using finite-element technique, *Comput. Fluids* 1 (1973) 73–89.
- [17] P.M. Gresho, R.L. Lee, R.L. Sani, On the time-dependent solution of the incompressible Navier–Stokes equations in two and three dimensions, in: *Recent Advances in Numerical Methods in Fluids*, Pineridge, Swansea, UK, 1980.
- [18] FIDAP Theoretical Manual, Fluid Dynamics International, Evanston, ILL, 1990.